Grid-interactive Efficient Buildings Using Thermal Energy Storage for Electric Heat Pumps

Prabhav AGRAWALA[1], Anurag GOYAL[2,*]

[1]Department of Mechanical Engineering, Malaviya National Institute of Technology, India

[2] Department of Mechanical Engineering, Indian Institute of Technology Delhi, New Delhi, India-110016
Contact Information: Ph- +91 11 26548574; Email- agoyal@mech.iitd.ac.in

* Corresponding Author

ABSTRACT

Electric heat pumps are a promising solution to decarbonize building heating by using renewable power and replacing existing fossil fuel based heating technologies. However, with the large-scale deployment of heat pumps, it is important to develop energy storage solutions to store renewable electricity and dispatch it when the generation is low, but the demand is high. This paper presents a system-level simulation of an air-to-water heat pump integrated with thermal energy storage for building heating. We coupled a validated quasi-steady thermodynamic model of the heat pump and a reduced-order transient model of a phase-change thermal storage module. We calculate the round-trip efficiency of the TES-integrated heat pump operating in the peak shaving mode using different TES materials for a representative commercial building. The performance of the proposed system showed a 26.67% reduction in the peak heating load in cold climates and the total electrical energy consumption for design day heating reduced by 4.8-11.5%. Our analyses show that a TES temperature close to the supply air conditions leads to a higher round-trip efficiency. Therefore, selecting a TES material based on its energy density (kJ/kg or kJ/m^3), phase-change temperature, and cost is crucial to successfully implementing these systems. The configuration of TES-integrated heat pumps and the heat transfer design of the TES module will be essential to reduce the peak heating energy demand and emissions and help buildings interact with the future electricity grid with a high fraction of renewable power.

1. INTRODUCTION

Space and water heating dominate the total energy consumption in buildings globally, amounting to almost 50% of the total consumption. In addition, fossil fuels (natural gas, propane, fuel oil) still meet more than 60% of this requirement. (IEA, 2022). Electric heat pumps are a promising solution to decarbonize building heating, and their deployment is increasing. Simultaneously, the fraction of renewable sources in our total energy generation and consumption is also increasing globally. Rapid adoption and deployment of renewable power are critically dependent on energy storage technologies because of the intermittent nature of solar and wind sources. Commercial and residential buildings can play an important role in limiting emissions from energy consumption.

The demand for heating in many buildings fluctuates asynchronously with renewable power generation, particularly solar photovoltaics. For instance, the heating demand in residential buildings is the lowest during the daytime and increases during the night and early morning hours. Commercial buildings also observe peak loads during early mornings when they need to be heated rapidly before the building users start occupying them. Moreover, operating heat pumps in cold climates can be challenging due to poor efficiency (or coefficient of performance, COP) at very low ambient temperatures. Thermal energy storage (TES) systems are one type of energy storage that can be employed in a distributed manner in buildings and enable energy storage during off-peak durations (low demand) and release at peak hours (high demand). TES systems can also help lower the capital cost of heat pumps by reducing the overall system size and providing ancillary benefits such as enhanced building energy efficiency and resiliency through interaction with a highly renewable grid (Mehling & Cabeza, 2008).

Several researchers have evaluated the performance of integrating active latent TES with air conditioning technologies (Moreno et al., 2014; Pardiñas et al., 2017). In general, active thermal energy storage systems utilizing phase change materials (PCMs) for latent energy storage are ideal for various climates (Y. Meng et al., 2021; Sultan et al., 2023). TES can be implemented in different operating modes, including load-shifting and load-shaving. Peak shaving allows greater operational flexibility with reported peak shaving values of even more than 50%; however, it generally comes at an increased cost of energy consumption during charging (Bruno et al., 2014).

Past research shows that the development of heat pump and TES models with adequate detail is crucial to analyze the performance of the combined system (Bordignon et al., 2024). Detailed models of heat pump systems based on field-data measurements and simulating flow and transient heat transfer physics at high spatial and temporal resolutions are very accurate but unsuitable for system-level analysis and parametric studies. Thus, many researchers have utilized idealized models using Carnot efficiencies or through curve-fitting field performance data (Hirschey et al., 2023; Sultan et al., 2023). These models can only be used to demonstrate the potential of ideal configurations or available commercial heat pumps, and are not suitable for estimating expected performance over a wide range of operating conditions. Moreover, limited research is available on integrating a realistic TES model with an overall heat pump simulation.

This paper presents detailed first principles based thermodynamic cycle model of an electric air-source heat pump (ASHP) coupled with a latent thermal energy storage (TES) module. The heat pump supplies hot water for building heating. We examine the peak-shaving and energy-saving potential of three different phase change materials using a round-trip coefficient of performance (COP). The TES model is a reduced-order transient heat transfer model that allows us to capture the effect of important material properties, including latent heat and phase-change temperature. We analyze the performance of the proposed system for a representative commercial building in very cold climates of the USA and estimate the potential of peak load shaving and energy savings.

2. METHODOLOGY

Figure 1 shows a schematic of the TES-integrated ASHP system. The heat pump supplies hot water for building heating. The hydronic loop couples the ASHP with the TES and the application (building). The direction of water flow through the TES module depends on whether the TES is being charged or discharged, which depends upon the hour of day (peak or off-peak hour). Finally, the room-side heat exchanger (application) supplies heat from the incoming water to the room air. We model the heat pump as a quasi-steady system using MATLAB® (The MathWorks Inc., 2022). We assume that the transient heat transfer effects are limited to the TES module only.

2.1 Model Inputs

2.1.1 Weather data and building load profile

We provide hourly weather data for the design heating day to our model. For this simulation, weather conditions at the beginning of the hour are assumed to remain the same until the start of the next hour. Our analysis mainly concerns using heat pumps in moderate to very cold climates. For this analysis, we selected Chicago, USA, and used Typical Meteorological Year (TMY3) weather data (NSRDB, 2022). We selected the coldest day of the year as the "design day" (Mitchell & Braun, 2012). Figure 2 (a) shows the hourly ambient temperature for the design day.

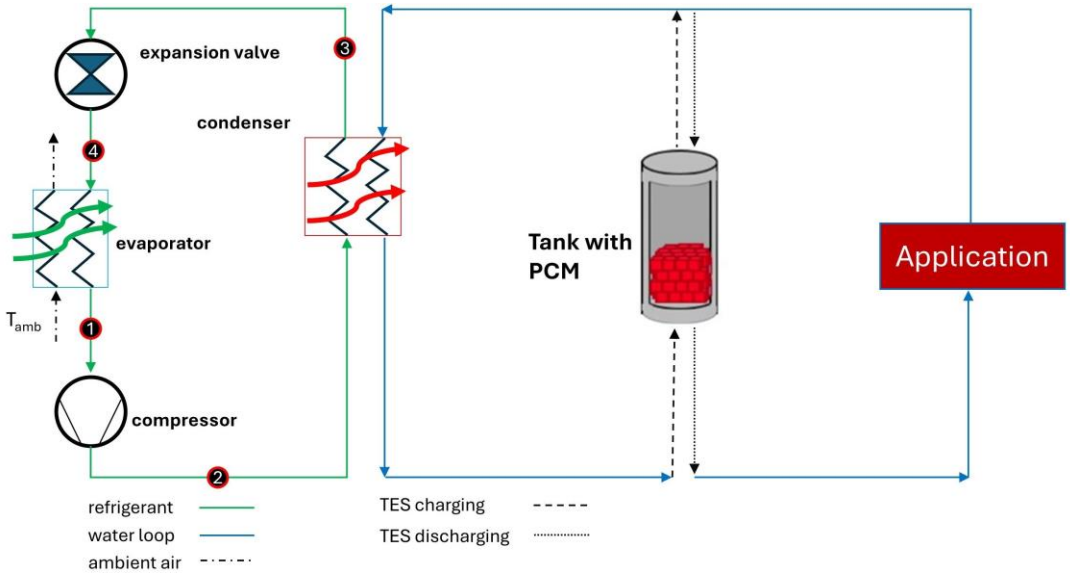

Figure 1: Schematic of ASHP with integrated phase-change TES module

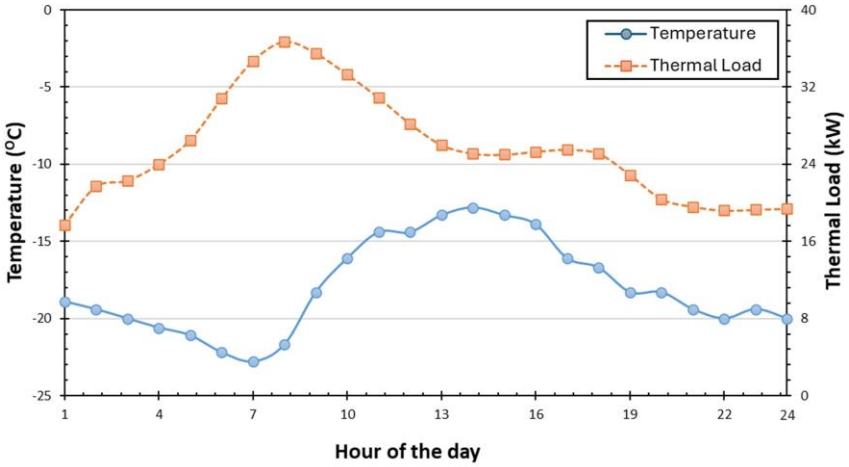

Figure 2: Heating design day ambient temperature for Chicago, USA (TMY3) and the load profile for a medium-office building normalized to 40 kW peak load

The next input to our model is the hourly building heating load profile, representing the thermal load that the ASHP+TES system must meet. We used published building load data for a "medium office building" in Chicago, USA (Wilson et al., 2022). The energy consumption data for thermal end-uses was filtered from the total energy consumption data and was processed using the reported heating conversion efficiencies (fossil fuel furnaces, district heating, ground-source heat pumps, electric heat pumps, etc.) to obtain an aggregated heating load profile for the design day (Figure 2(b)). We normalized the load profile to a peak load of 40 kW, and a representative floor area of 929 m^2 (10,000 ft^2). We designed the TES-integrated ASHP to operate at 5% above the average building thermal load on the design day, i.e., 29.32 kW (8.34 TR). The extra 5% capacity will ensure that the load is met at all times of the design day. When the instantaneous thermal load is lower than this fixed ASHP output, the TES module stores the excess heating and discharges it during peak hours when the building load exceeds the fixed ASHP capacity. For the peak load of 40 kW, the fixed ASHP output of 29.32 kW represents a peak shaving of 26.7%, provided that the TES module can store excess energy and discharge it at a sufficient rate to meet the loads.

2.2 Systems-Level ASHP Model

We developed the thermodynamic model of the TES-integrated ASHP system in MATLAB®. We used the following simplifying assumptions:

(a) Steady-state operating conditions in the heat pump cycle.
(b) Negligible pressure drops in all heat exchangers.
(c) Isenthalpic expansion of the refrigerant in the throttling valve.
(d) 5°C of superheating and subcooling in the evaporator and condenser, respectively.
(e) No heat losses in any component of the system.
(f) Negligible auxiliary power for pumps and fans.
(g) The closest approach temperatures (CATs) of all water-cooled and air-cooled heat exchangers are set to 10°C and 5°C, respectively.
(h) TES module operates at a best-case CAT of 1.5°C.
(i) No sensible heat is exchanged in the TES module, i.e., it always remains at the PCM transition temperature.

Based on commercial heat pump specifications, we used R32 refrigerant in the simulation and use REFPROP® to determine refrigerant properties (Lemmon et al., 2018). We set the compressor to operate at a single speed with a fixed isentropic efficiency of 72%. The methodology for heat pump simulation is adapted from the chiller model developed by Bhattacharyya and Goyal (2024). We establish the energy balance equations for each component, with the outlet state of one component becoming the inlet state of the downstream component. The initial assumptions of CATs in different components allow us to completely define the thermodynamic state of the refrigerant at the condenser outlet and evaporator inlet. Using superheating/subcooling and the compressor efficiency, coupled with standard heat pump rating conditions (AHRI, 2023), we estimate the condenser and evaporator heat transfer rates and overall heat transfer conductances and the system COP.

2.2.1 Validation of baseline ASHP model

We validated the thermodynamic model of the ASHP described in the previous section using field data reported by Gibb *et al.* (2023). Their work included field performance data of various ASHPs at low temperatures (between 0°C and -30°C) in countries with a predominantly cold climate. For 2,760 measurements of the COP of approximately 550 systems, the average COP was 2.74 for temperatures between 5°C and -10°C. Our model predicted the average COP for the same temperatures to be 2.91, marginally higher than the reported value (by 6.2%).

2.3 Integration of TES and the operation scheme

2.3.1 System configuration

For this study, we consider the TES module to be a standalone tube-in-tank type heat exchanger, as presented by Meng and Zhang (2017). The TES module is connected to the room-side HX and the hydronic loop of the ASHP. The tank is filled with a PCM which can melt (charge) or freeze (discharge). PCMs have a high phase-change enthalpy, making them a preferred choice for TES systems. (Osterman & Stritih, 2021). The overall schematic of the system is shown in Figure 1. This configuration provides flexibility in buildings with space constraints because the TES module can be a drop-in addition to the overall HVAC system.

2.3.3 TES control scheme

There are two main schemes of TES operation: load shaving and load shifting. We chose the load-shaving scheme because it allows for a relatively smaller TES module size and different operating modes for greater operational flexibility. In this configuration, the ASHP operates at a set output heating value (29.32 kW), irrespective of the thermal load to be met by the system. During off-peak hours (when the building thermal load is less than the ASHP output), excess thermal energy is used to melt the PCM in the TES module and charge it. During peak hours, the flow of water through the TES module is such that it absorbs thermal energy from the module, freezing it and, therefore, discharging the system. During peak hours, the thermal load is met by the combined output of the ASHP and the TES.

2.3.4 Mathematical Modeling

We implement standard rating conditions from AHRI 550/590 standard for water-cooled condensers during the discharging mode of the system (AHRI, 2023). The mass flow rate of the condenser water is set to 2.62 kg s^{-1}. The temperature of the water leaving the condenser is fixed to T_{PCM} + 2.5°C (non-standard value) during the first time step of the charging and a constant temperature of 45°C (within the expected range for standard ASHP operation) during discharging. Since the ASHP (condenser) heat output is fixed, the water temperature at the inlet of the condenser is calculated. In the TES module, we assumed a minimum approach temperature (CAT) of 1.5°C for the water leaving the module, during both processes. This CAT gives the best-case temperature of the water leaving the module, representing the maximum possible heat transfer rate in the module. This best-case water temperature, in conjunction with the water temperature at the condenser outlet, is used to find the log-mean temperature difference (*LMTD*) in the module, and hence the maximum possible overall conductance (for charging and discharging), using Equation (1):

$$\dot{Q}_{max} = UA_{TES,max} LMTD \quad (1)$$

Here, $\dot{Q}_{max}$ is the maximum possible heat transfer rate from the TES module during the charging and discharging processes, depending on the hour of the day. During charging, the maximum possible heat transfer rate is the difference between the fixed condenser output and the minimum heating load at any instant during the charging process. On the other hand, during discharging, the maximum possible rate of discharge is the difference between the fixed condenser output and the maximum heating load on the system at any instant during the discharging process. This maximum possible heat transfer rate may or may not be achievable in the TES module depending on the amount of stored thermal energy relative to the maximum storage capacity (state of charge, *SOC*). Therefore, we use a time-dependent decay function to calculate the actual heat transfer conductance (UA_{TES}) based on the instantaneous state of charge (*SOC*) and the previously calculated maximum conductance from Equation 1. The time-dependent *UA* functions for charging and discharging are given by Equations 2 and 3, respectively:

$$UA_{ch} = UA_{ch,max}\{1 - SOC[1 - e^{\frac{-t_{ch}}{\tau_{ch}}}]\} \quad (2)$$

$$UA_{dis} = UA_{dis,max}\, SOC\, e^{\frac{-t_{dis}}{\tau_{dis}}} \quad (3)$$

Here, t_{ch} is the time instant during charging and τ_{ch} is the time constant based on the total charging duration (number of off-peak hours). Similarly, t_{dis} and τ_{dis} represent the time instant during discharging and the time constant based

on the total discharging duration. The overall heat transfer conductance values obtained using the above procedure are then used to find the actual heat transfer rate $\dot{Q}_{actual}$ in the TES at any instant during the charging or discharging process:

$$\dot{Q}_{actual} = UA_{ch/dis}LMTD \quad (4)$$

The available heat transfer rate ($\dot{Q}_{available}$) is defined as the difference between the ASHP output and the thermal load at any given time. The final heat transfer rate ($\dot{Q}_{final}$) in the TES is the minimum of two heat transfer rates: $\dot{Q}_{available}$ and $\dot{Q}_{actual}$.

In the supply side HX, the temperature of the air entering and leaving the HX is assumed to be at the setpoint temperature of the room (35°C), and using a fixed water temperature difference of 7°C, the inlet and outlet water temperatures are calculated. At the end of the simulation, we calculate the round-trip COP, which is defined based on the total heating output and energy consumption for the day, and compare the total compressor power use for the day.

3. RESULTS AND DISCUSSION

3.1 Benchmarking of TES-integrated ASHP system

This section explains how the ASHP-TES system was benchmarked against baseline ASHP systems without TES. The weather and load profiles shown earlier were used to run the baseline simulation at a room setpoint temperature of 21.12°C. The corresponding supply temperature of the air in the application is fixed at 35°C. The water supply temperature in the application heat exchanger corresponding to this supply air temperature is calculated to be 45°C. These values are representative of real systems, ASHP testing standards, and field data (Johnson, 2013).

For a design day simulation, we recognized that a fixed-capacity ASHP could not track the variable heating load perfectly. We implemented a duty-cycle-based control scheme that turns off the compressor at certain times of the day. These points are then designated as 'compressor-off' hours. These hours are excluded in the final calculation of the total energy consumption, yielding a more realistic COP estimate. Using this method, we obtained a round-trip COP of 2.30 for the baseline system. The lowest and highest values of the instantaneous COP for this system were 2.44 and 2.17, respectively.

3.2 Heating design day analysis

3.2.1 Selection of PCM

The choice of the PCM dictates the peak demand reduction and energy-saving potential of the system. Hirschey *et al.* (2023) recommended keeping the PCM transition temperature as close as possible to the application temperature for maximum energy savings. During charging, the heat pump must supply heat at a temperature that is higher than the PCM transition temperature, which is generally higher than the application temperature. Thus, compared to the baseline system, the power consumption increases and the COP decreases during charging. In addition to the transition temperature, the phase change enthalpy and mass density of a PCM are also important factors in selecting an appropriate PCM. These two parameters directly influence the volume of the TES module when placed on-site. Paraffin wax is a common material for hot TES and is readily available in a variety of compositions, making it possible to study and choose a suitable transition temperature. Thus, we choose n-Tetracozane (T_{PCM} = 50.6 ^{O}C) as a material for our first analysis (Alva et al., 2017).

3.2.2 Peak shaving fraction and energy savings

Figure 3 compares the performance of the TES-integrated ASHP system with the baseline system throughout the day. Figure 3(a) shows different heat transfer rates in the two systems, and Figure 3(b) shows the variation of the input compressor power and the COP. Implementing a duty-cycle-based operation scheme for the baseline system (without TES) meant that the compressor automatically turned off at certain hours during the day. This is shown in Figure 3. While the total compressor energy consumption has reduced by 9.30% using TES (331.62 kWh, down from 365.6 kWh), the average COP has also reduced to 2.13 from 2.30. This is because the system supplies heat at a significantly higher temperature throughout the day and operates continuously, unlike the baseline system, which uses a duty-cycle-based control scheme. Building load profile and the peak shaving fraction significantly affect the total energy savings and COP of the TES-integrated ASHP.

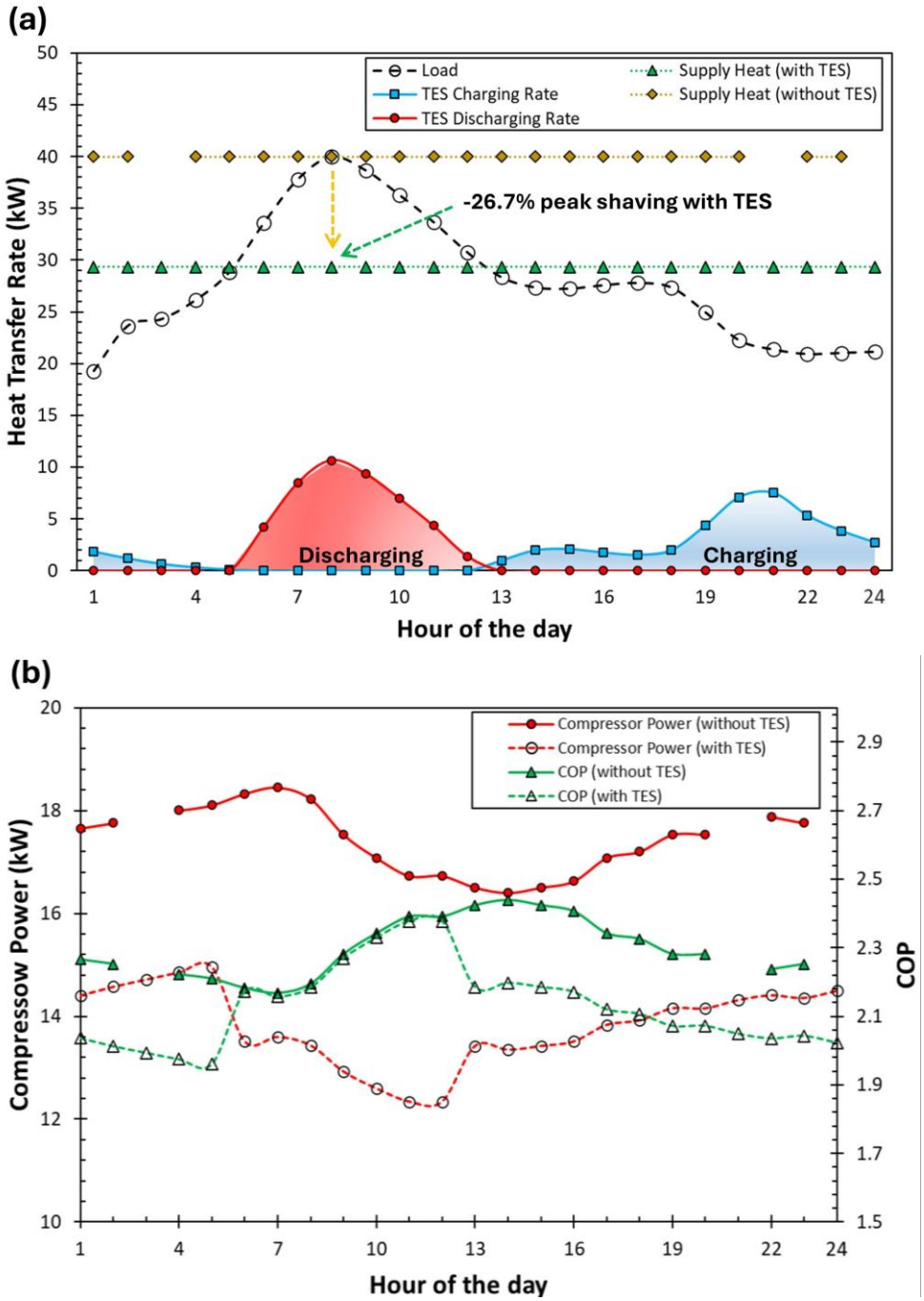

Figure 3: (a) Heat transfer rates for TES-integrated and baseline ASHP, (b) hourly compressor power and COP

3.3 Effect of PCM transition temperature

We studied the effect of the transition temperature of the PCM on the overall system performance (Figure 4 and Table 1). We selected three different paraffin wax-based PCMs: n-trikozane, n-tetracozane, and n-hexacozane corresponding to transition temperatures (T_{PCM}) of 47.5°C, 50.6°C, 56.3°C, respectively. Figure 4(a) shows the total power consumption using three different PCMs. The distinction between the charging and discharging phases is also shown. Figure 4(b) shows the variation of the COP throughout the day.

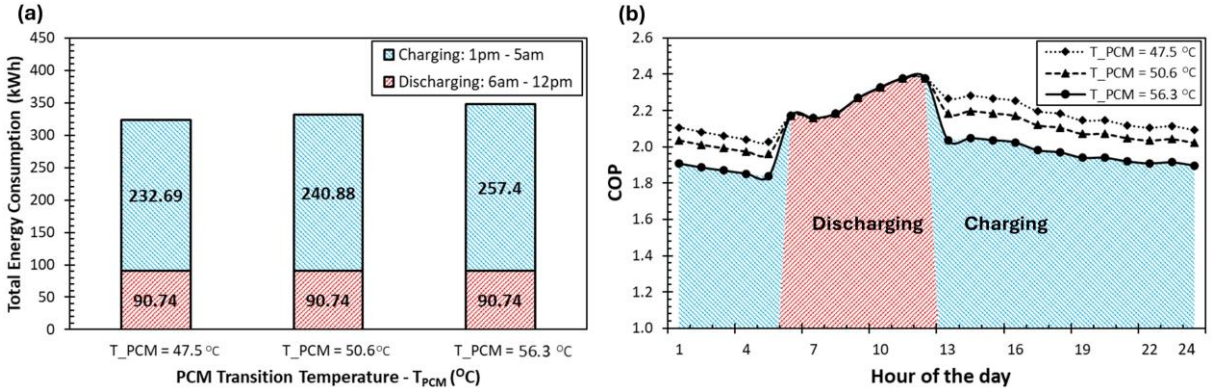

Figure 4: Effect of PCM transition temperature on system performance (a) total power consumption, and (b) COP

Since we set a constant water discharge temperature at the condenser outlet during discharging, the power consumption and COP values are independent of the PCM. During the charging phase, the energy consumption is directly proportional to the transition temperature because the water discharge temperature at the condenser outlet is 2.5°C above the PCM transition temperature. Thus, even though the system shifts the same amount of energy into the PCM, it must do so at a higher temperature, leading to higher energy consumption by the compressor and reduced COP values. The round-trip COP values obtained for the three different materials are 2.18, 2.13, and 2.04 (in the order of increasing PCM transition temperature). While these are all lower than the baseline value of 2.30, the total compressor energy consumption is lower than the baseline energy consumption by 5.2-11.3%. However, if the total compressor energy consumption during the peak hours (TES discharging) only is considered, it is reduced by 26.67% for all three PCMs.

Table 1: Effect of PCM transition temperature

PCM	PCM Transition Temperature - T_{PCM} (°C)	Total Compressor Energy Consumption (kWh)	Round-trip COP
n-trikozane	47.5	323.42 (↓11.54%)	2.18 (↓5.22%)
n-tetracozane	50.6	331.62 (↓9.30%)	2.13 (↓7.39%)
n-hexacozane	56.3	331.62 (↓4.78%)	2.04 (↓11.30%)

4. CONCLUSIONS

In this work, we developed a thermodynamic model of a TES-integrated ASHP system for peak-load shaving for building heating. We studied the load-shaving characteristics and energy consumption of three different PCMs and compared to a baseline system without TES, using real weather and thermal load data. We show a peak-load shaving value of 26.7%. The use of TES reduced the peak electric power consumption by 26.28%. The total energy consumption by the compressor reduced by 4.78%-11.54% for the simulated materials. The round-trip COP of the baseline system for the design day is estimated at 2.30, higher than the TES-integrated ASHP system, which varied between 2.04-2.18 as the PCM transition temperature was decreased. Our analyses show that the

Our model can be used for annual simulations to evaluate the energy-savings potential and economic feasibility of TES-integrated electric heat pumps for residential and commercial buildings in different climate zones. It would also allow for detailed parametric studies to study the effect of multiple variables, such as heat pump configurations and TES materials, and develop appropriate control schemes, and enable more intelligent design of systems for grid-interactive buildings. Future work includes analyzing the building typologies that would benefit the most from adopting TES with heat pumps and optimizing the PCMs.

NOMENCLATURE

T	temperature	(°C)
UA	thermal conductance	(W/m-K)
$\dot{Q}$	heat transfer rate	(W
t	process time instant	(s)

τ	process time constant	(s)

Subscript

PCM	phase change material
ch	charging
dis	discharging
max	maximum

REFERENCES

AHRI. (2023). *ANSI/AHRI Standard 550/590-2023 (I-P)*.

Alva, G., Liu, L., Huang, X., & Fang, G. (2017). Thermal energy storage materials and systems for solar energy applications. *Renewable and Sustainable Energy Reviews*, *68*, 693–706. https://doi.org/10.1016/j.rser.2016.10.021

Bhattacharyya, S., & Goyal, A. (2024). Energy saving potential of phase-change thermal energy storage for cooling in buildings. *(In Review)*.

Bordignon, S., Spitler, J. D., & Zarrella, A. (2024). Simplified water-source heat pump models for predicting heat extraction and rejection. *Renewable Energy*, *220*, 119701. https://doi.org/10.1016/j.renene.2023.119701

Bruno, F., Tay, N. H. S., & Belusko, M. (2014). Minimising energy usage for domestic cooling with off-peak PCM storage. *Energy and Buildings*, *76*, 347–353. https://doi.org/10.1016/j.enbuild.2014.02.069

Gibb, D., Rosenow, J., Lowes, R., & Hewitt, N. J. (2023). Coming in from the cold: Heat pump efficiency at low temperatures. *Joule*, *7*(9), 1939–1942. https://doi.org/10.1016/j.joule.2023.08.005

Hirschey, J., Li, Z., Gluesenkamp, K. R., LaClair, T. J., & Graham, S. (2023). Demand reduction and energy saving potential of thermal energy storage integrated heat pumps. *International Journal of Refrigeration*, *148*, 179–192. https://doi.org/10.1016/j.ijrefrig.2023.01.026

IEA. (2022). *The Future of Heat Pumps*. www.iea.org

Johnson, R. K. (2013). *Measured Performance of a Low Temperature Air Source Heat Pump* (NREL/SR--5500-56393, DOE/GO--102013-3788, 1260317; p. NREL/SR--5500-56393, DOE/GO--102013-3788, 1260317). https://doi.org/10.2172/1260317

Lemmon, E. W., Bell, I. H., Huber, M. L., & McLinden, M. O. (2018). *NIST Standard Reference Database 23: Reference Fluid Thermodynamic and Transport Properties-REFPROP, Version 10.0* [Computer software]. National Institute of Standards and Technology, Standard Reference Data Program. https://doi.org/10.18434/T4/1502528

Mehling, H., & Cabeza, L. F. (2008). *Heat and cold storage with PCM*. Springer Berlin, Heidelberg. https://doi.org/10.1007/978-3-540-68557-9

Meng, Y., Sheng, L., & Zhao, Y. (2021). Techno-economic analysis of air source heat pump combined with latent thermal energy storage applied for space heating in China. *Applied Thermal Engineering*, *185*, 116434. https://doi.org/10.1016/j.applthermaleng.2020.116434

Meng, Z. N., & Zhang, P. (2017). Experimental and numerical investigation of a tube-in-tank latent thermal energy storage unit using composite PCM. *Applied Energy*, *190*, 524–539. https://doi.org/10.1016/j.apenergy.2016.12.163

Mitchell, J. W., & Braun, J. E. (2012). *Principles of Heating, Ventilation, and Air Conditioning in Buildings*. John Wiley & Sons.

Moreno, P., Solé, C., Castell, A., & Cabeza, L. F. (2014). The use of phase change materials in domestic heat pump and air-conditioning systems for short term storage: A review. *Renewable and Sustainable Energy Reviews*, *39*, 1–13. https://doi.org/10.1016/j.rser.2014.07.062

NSRDB. (2022). *TMY Weather Data*. National Renewable Energy Laboratory (NREL). https://nsrdb.nrel.gov/

Osterman, E., & Stritih, U. (2021). Review on compression heat pump systems with thermal energy storage for heating and cooling of buildings. *Journal of Energy Storage*, *39*, 102569. https://doi.org/10.1016/j.est.2021.102569

Pardiñas, Á. Á., Alonso, M. J., Diz, R., Kvalsvik, K. H., & Fernández-Seara, J. (2017). State-of-the-art for the use of phase-change materials in tanks coupled with heat pumps. *Energy and Buildings*, *140*, 28–41. https://doi.org/10.1016/j.enbuild.2017.01.061

Sultan, S., Hirschey, J., Kumar, N., Cui, B., Liu, X., LaClair, T. J., & Gluesenkamp, K. R. (2023). Techno-Economic Assessment of Residential Heat Pump Integrated with Thermal Energy Storage. *Energies*, *16*(10), Article 10. https://doi.org/10.3390/en16104087

The MathWorks Inc. (2022). *MATLAB version 9.13.0*. The MathWorks Inc.

Wilson, E. J. H., Parker, A., Fontanini, A., Present, E., Reyna, J. L., Adhikari, R., Bianchi, C., CaraDonna, C., Dahlhausen, M., Kim, J., LeBar, A., Liu, L., Praprost, M., Zhang, L., DeWitt, P., Merket, N., Speake, A., Hong, T., Li, H., … Li, Q. (2022). *End-Use Load Profiles for the U.S. Building Stock: Methodology and Results of Model Calibration, Validation, and Uncertainty Quantification* (NREL/TP-5500-80889). National Renewable Energy Lab. (NREL), Golden, CO (United States). https://doi.org/10.2172/1854582

ACKNOWLEDGEMENT

The authors gratefully acknowledge the financial support for this work through the Science and Engineering Research Board (SERB), Government of India (Grant# SRG/2022/001778), and ITC Limited (Project# RP04317). The authors also acknowledge the help from Vaishnavi Gupta in analyzing the load profile data.